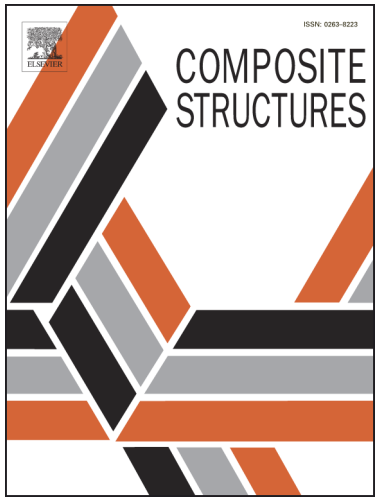

Investigation into Skin Stiffener Debonding of Top-Hat Stiffened Composite Structures

J.E. Yetman, A.J. Sobey, J.I.R. Blake, R.A. Shenoi

PII: S0263-8223(15)00525-5
DOI: http://dx.doi.org/10.1016/j.compstruct.2015.06.061
Reference: COST 6560

To appear in: *Composite Structures*

Please cite this article as: Yetman, J.E., Sobey, A.J., Blake, J.I.R., Shenoi, R.A., Investigation into Skin Stiffener Debonding of Top-Hat Stiffened Composite Structures, *Composite Structures* (2015), doi: http://dx.doi.org/10.1016/j.compstruct.2015.06.061

INVESTIGATION INTO SKIN STIFFENER DEBONDING OF TOP-HAT STIFFENED COMPOSITE STRUCTURES

J.E. Yetman[a,1,**], A.J. Sobey[a,1], J.I.R. Blake[a,1], R.A. Shenoi[a,1]

[a] *Fluid Structure Interactions, University of Southampton, University Rd, Southampton SO17 1BJ, England, UK*

Abstract

Top-hat stiffened plates provide an efficient structure for engineering applications. During service debonding between the stiffener and the plate is often observed and parametric studies of open section stiffeners have shown that debond size and location have a significant effect on the damage mode of the panel. However, these studies do not consider the interaction of failure modes and do not assess the ultimate failure of the structure. In this paper top-hat stiffened composite structures are assessed considering debond damage between the stiffener and plate. A non-linear finite element model is used to perform a parametric study on the effect of both damage and the panel's geometry on the failure modes, ultimate strength and its damage tolerance. Results show that top-hat stiffened panels exhibit a trend between ultimate strength and the debond size with crack initiation not necessarily propagating. Geometric imperfections accelerate buckling but can provide an arrest point for crack propagation.

Keywords: Damage Tolerance, Delamination, Stiffened Structures, Progressive Damage

1. Introduction

Defects and damage events are likely to occur within the lifetime of structures. It is imperative that once damage has occurred it can be rapidly assessed and suitable precautions taken to ensure safety of the structure and its users, this must be done cost efficiently. To optimise maintenance and reduce costs it is also imperative to know if damage must be fixed immediately, in the near future or if it poses no current threat.

*Corresponding author. Tel.: +442380594763
**Principal corresponding author
Email address: J.E.Yetman@Soton.ac.uk (J.E. Yetman)
[1] This is the specimen author footnote.

Many authors have investigated damage progression in previous intact structures with good correlation to experimental results. However, there is still limited research conducted on the residual capabilities of structures containing prior delaminations and associated damage. Falzon [1] showed that mid bay delaminations and holes had minimal effect on the ultimate collapse load of a stiffened structure; however it has been shown by Meeks et al. [2], Yap [3, 4] and Wiggenraad et al. [5] that delaminations present under the stiffener have a significant effect on the ultimate strength of the panel. Wiggenraad et al. [5], Suh [6], Meeks et al. [2], Orifici et al. [7] and Riccio et al. [8] investigated impacted I and T stiffened panels experimentally and demonstrated modelling capability. Parametric studies have shown that debond size and location have a significant effect on the damage mode of the panel[3, 4, 9, 10]. However these parametric studies do not consider the interaction of failure modes as they omit material failure or damage propagation and therefore do not assess the ultimate failure of the structure.

Research on damaged stiffened structures to date has primarily focused on T-stiffeners rather than closed section stiffeners. Work on top-hat stiffeners by Sumpter [11] and Falzon [1] investigated the effect of mid-bay delaminations and circular cut-outs respectively however, damage to the stiffener-plate interface is not covered in the literature. Top-hat stiffeners are used extensively in the aerospace, civil and marine industries as they provide increased torsional rigidity compared to open section stiffeners providing increased resistance to buckling modes. The most common form of reinforcing fibre is E-glass used in polymer matrix composites which provides a cost effective solution for many applications. This paper assesses the effect of skin stiffener debonding in top-hat stiffened panels, as there is a lack of research on the damage response of top-hat stiffened panels, investigating both debond size and location and geometric parameters. A non-linear finite element model, incorporating both material degradation and debond crack propagation, is used to assess the effect of damage within the stiffened panel and the ultimate collapse strength.

2. Modelling Methodology

A generic glass-vinylester top-hat stiffened panel is considered under compressive loading. Debond growth, inter-frame and frame buckling leads to an interaction of damage mechanisms therefore, a multi-stiffened panel is considered with a damaged zone in the region of the central stiffener between the stiffener flange and plate.

2.1. Panel Configuration

A stiffened panel is considered with dimensions shown in figure 1. The panel is loaded in longitudinal compression with the loaded and reaction ends of the panel fully clamped. It is considered to be part of a larger grillage and therefore symmetric boundary conditions are applied to the unloaded transverse edges. The boundary conditions and mesh density, which is discussed in section

2.4, are shown in figure 2. The plate and stiffener webs are a balanced glass-vinylester woven roving (WRE580) aligned with the stiffener direction where the table of the stiffener contains an additional central glass-vinylester unidirectional ply (UE500). Cohesive elements are used at the interface with a depth of 0.01mm. The material properties and cohesive element propertiesare shown in table 1. The Benzeggagh-Kennane exponent [12] is calculated at 1.17 using the least squares fitting method through available data. This gives an R^2 value of 0.9242 showing a reasonable fit.The shear interface strengths are taken as 23.2MPa which represents the lower range of material parameters reported by Juntikka and Olsson [13]. The normal interface strength is taken as the transverse strength of the unidirectional laminate as the tensile failure of the fibre-resin interface represents the mode of failure in this test.

2.2. Definition of Failure Mechanisms

To assess the onset of buckling a study has been conducted which assesses the buckling point of the plate based on the deflection at the centre of the plate. The plates' out-of-plane deflection is compared against the end shortening for increasing debond size with a central debond and a nominal imperfection. For the intact case the deflection curve shows that the plate exhibits a linear increase in out-of-plane deflection until a marked change in out-of-plane deflection with end shortening is observed. A similar trend is observed for the damaged case under a negative inflection however, for a positive inflection but the buckling point is less clear in this case. Based on these studies end shortening of greater than 0.05 is chosen to represent the 'local plate buckling' point as it was shown to give reasonable results when considering both the out-of-plane deflection for negative and positive buckled inflections. Similarly the out-of-plane deflection is monitored on the table of the stiffener to determine 'stiffener buckling' and the plate in the centre of the flange to determine 'local plate buckling' with both longitudinally positioned at the centre of the debond. As buckling can be defined as a marked change in stiffness 'panel buckling' is recorded at 5% change in stiffness which represents a marked change panel stiffness for the intact case. Significant 'damage initiation' is defined when 100 elements, in either the plate or the stiffener, exceed the Tsai-Wu failure criterion. 100 elements are chosen as this is a significant area relative to the mesh size. Debond 'Crack initation' is defined as a single cohesive element reaching 99% degradation in stiffness. The load deflection curve is monitored and the analysis is stopped when a 20% reduction in load is observed, which corresponds to gross failure or global buckling of the panel. The maximum recorded load is defined as the 'ultimate load'.

2.3. Modelling Methodology

The model, which accounts for both geometric and material nonlinearities, is implemented in ABAQUS using IRIDIS the High Performance Computing Facility at Southampton University. An automated script is used to generate an equivalent single layer approach from 8 node shell elements (S8) minimizing

the computational effort required whilst providing an accurate assessment of the post-buckled response of the stiffened plate. The stiffeners, plate and cohesive interface are connected by multi-point constraints which restrict the degrees of freedom of the plate nodes to that of the connected flange nodes. To initiate the post-buckled state an imperfection is seeded using the primary buckled mode of the intact case found via Eigenvalue analysis as illustrated in figure 3. A nominal out-of-plane imperfection, 0.1% plate thickness, is used which does not affect the overall buckled and post-buckled mode shape. A forced imperfection, 10% plate thickness, is also assessed as observed in large scale manufacture measured by Smith [14].

A non-linear analysis is conducted using a user-defined material to implement a strength based progressive damage methodology incorporating the Tsai-Wu failure criterion. Following the onset of failure the material properties of the affected element are instantaneously degraded to 1% of the nominal value depending on the failure mode as shown in table 2.

To avoid numerical convergence issues a viscous regularization scheme is applied; an artificial Duvaut and Lions [15] viscous model is used which causes the tangent stiffness matrix of the softening material to be positive for sufficiently small time increments, as shown by equation 1.

$$\dot{d_v} = \frac{1}{\eta}(d - d_v) \tag{1}$$

where η is the viscosity parameter and is chosen to optimise convergence without affecting the panel response, d is the degradation factor and d_v is the regularised degradation factor.

The crack propagation is assessed using a linearly degrading cohesive element with traction separation response shown for a single mode in figure 4. G_c is the critical strain energy release rate, K_i the interfacial initial stiffness and t_o is the interfacial strength. The cohesive element model approach allows for viscous damping of these elements. Numerical instabilities were not found using viscous damping of 1E-6 for both material damage propagation and crack propagation which was shown not to affect the load-deflection response, damage properties, buckling onset or post-buckling behaviour.

A comprehensive review of damage initiation criterion compared to mixed mode experimental data is lacking in the literature and these criterion are not fully compared or validated. Therefore, the most commonly used criterion is adopted to assess the location and load at which the debond initiates; the quadratic nominal stress criterion [16] as shown in equation 2 where σ_{3T}, σ_{23} and σ_{33} refer to the out-of-plane tensile stress and shear stresses repectively and S_{3T}, S_{23} and S_{33} the equivalent strengths.

$$\left(\frac{\sigma_{3T}}{S_{3T}}\right)^2 + \left(\frac{\sigma_{32}}{S_{32}}\right)^2 + \left(\frac{\sigma_{31}}{S_{31}}\right)^2 \geq 1 \tag{2}$$

Under mixed mode loading the Benzeggagh-Kenane criterion [12] shown in equation 3 is used to assess the mixed mode failure criterion. η_{BK} is a semi-

empirical exponent applied to delamination iniation and growth and $G_T = G_I + G_{II} + G_{III}$.

$$G_{IC} + \left((G_{IIC} - G_{IC}) \frac{G_{II}}{G_T} + (G_{III} - G_{IC}) \frac{G_{III}}{G_T} \right) \left(\frac{G_{II} + G_{III}}{G_T} \right)^{\eta_{BK}-1} \geq G_T \tag{3}$$

2.4. Convergence

Convergence of the model is checked for the damaged case for a central debond of 350mm. The effect of decreasing mesh size on the ultimate load, damage initiation, debond crack initiation and buckling load is assessed both for decreasing shell element size and number of cohesive elements; a trial was performed using two sizes of elements, chosen so that 2 or 3 elements fit within the characteristic length (Ne), and the results compared in figure 5. Figure 2 shows the mesh density and highlights the cohesive elements in more detail in the region of the debond area. Convergence is achieved for the damage initiation and buckling load for a shell element size of 5mm or less. The ultimate load is converging and shows a 1.8% reduction from a shell element size of 5mm to 2.5mm. The debond crack initiation load shows more variation as the shell element reduces. This is partly due to its occurance at the stress singularity; as the element size reduces, the load to cause degradation of a single element also decreases. It is therefore unlikely that this measure would truly converge. 5mm shell elements with 2 elements in the cohesive zone are chosen as good convergence is shown as this selection suitably accounts for the post-buckled response of the intact and damage size considered here.

2.5. Model Verification

There is a lack of experimental data with concise material properties and array of failure combinations for compressively loaded multi-stiffened panels containing debond damage it is necessary to verify the individual components of the model separately. Solutions are compared to experimental and numerical results in the literature. The buckled and post-buckled response of more stiffened structures is verified against experimental work of Kong et al. [17]. The cohesive element crack propagation method is verified against experimental results of mode I and mode II tests by Reeder et al. [18]. The inclusion of delaminations in composite structures is verified against through width delamination tests conducted by Kutlu and Chang [19]. These elements are combined in a final study to investigate the progressive collapse of an intact top-hat stiffened structure against full scale tests conducted by Smith [14].

2.5.1. Buckling of Stiffened Plates

The buckled and post-buckled responses of stiffened structures are verified against experimental work of Kong et al. [17] who studied a composite panel

stiffened with two longitudinal blade stiffeners under in-plane compressive loading. The instantaneous degradation model is used with a combined failure criterion of the world wide failure exercise recommended criterion for unidirectional lamina; Puck, Tsai-Wu, and Zinoviev Soden et al. [20]. The newly developed model has shown good correlation to the post-buckled response; qualitatively the model matches the experimental observations well; matching the buckled mode shape and failure modes observed. Figure 6 shows the predicted buckled mode shapes in the proposed model and Kong's model which show good correlation. Figure 7 shows predicted load shortening curves compared to the experimental data of Kong et al. [17]. Quantitatively the model overestimates both the buckling load and final failure load by 20% and 18% respectively. The initial stiffness is also slightly overestimated and therefore it is assumed that the material properties quoted by the author are not a true representation of the build quality. The failure mode is strongly affected by the deformation of the stiffeners and the post-buckled state therefore, the boundary condition on the stiffener ends is critical in accurately modelling failure and is difficult to assess without further experimental data. Based on the assumptions made, the model is thus deemed to be well verified.

2.5.2. Mode I and II Crack Propagation

The crack initiation and propagation methods are verified against experimental results of mode I, double cantilever beam, and mode II, end notch failure coupon, tests conducted by Reeder et al. [18]. The load displacement curves are compared to the experimental data for the DCB and ENF tests shown in figure 8. The model, using material properties stated by Reeder et al. [18], shows good correlation with the experimental results for crack propagation in modes I and II can be obtained from the cohesive element method using shell elements in a 3D model. For both mode I and II tests the initial stiffness is accurate. In mode I the model underestimates the peak load by 7%, experimentally fibre bridging may be present behind the crack tip. The mode II response including the stiffness degradation due to a gradual build of matrix cracks and damage at the crack tip prior is well captured, although the peak load is underestimated by 13%.

2.5.3. Through Width Delaminations

The model's ability to follow combined crack propagation and buckling is verified against the experimental work of Kutlu and Chang [19]. Composite coupons are loaded in compression containing through width delaminations positioned centrally across the coupon. Figure 9 shows the boundary conditions and the good correlation between the buckling mode of Kutlu and Chang's in comparison to the proposed model. . Figure 10 shows the load-strain response for the upper delaminated ply and the lower laminate, where strain is measured at a central location on the outer surfaces. The initial stiffness, buckling load of the delaminated ply and transition to the post-buckled state are well captured by the model; shown by the linear load strain response up to a load of 6kN and the transition from negative to positive strain on the outer edge of the front

ply. However, the global buckled response and ultimate collapse is significantly over estimated by the model. The maximum load, which is coincident with the global buckling load, is predicted at 13.9kN representing an overestimation by 32%. This overestimation may be attributed to unrealistic boundary condition assumptions which are assumed to be clamped whereas the experimental fittings are unlikely to restrict all rotations and would lead to increased deflection of the back laminate.

Figure 11 compares the deflection at the center of the front and back plies against applied load for the current three dimensional shell element method and is compared to the 2D numerical models of Liu and Zheng [21] and finite strip method implemented by Zhang and Wang [22]. The current three dimensional shell element model shows good overall correlation with the alternative methodologies; all three numerical models overestimate the global buckling load confirming that this is due to unrealistic boundary condition assumptions, imperfections or flaws within the material.

2.5.4. Damage Evolution in Top-Hat Stiffened Panel

The damage progression in top-hat stiffened composite structures is used to verify delamination initiation and propagation in a post-buckled structure against full scale tests conducted by Smith [14] on a MCMV deck structure. A single stiffener parallel to the loading direction and located at the center of the grillage is modeled using symmetric boundary conditions on the unloaded edges and clamped condition on the loaded and reaction edges.

The maximum out-of-plane displacement with increasing load is shown in figure 12 comparing the experimental data and the modelling methodology. Quantitatively the initial stiffness, buckling load and plate deformation are reasonably captured by the model given the boundary condition assumptions. The cohesive stress criterion is reached at 605kN and the first element degrades by 95% at 796kN on the anti-node line and at the central inner inner flange. Unstable crack propagation develops at 1310kN. Delamination initiation is predicted experimentally at 920kN. Smith et al. observed a residual capability following delamination propagation leading to ultimate failure at 1090kN.

As the models ability to assess the post-buckled deformation and damage progression has been previously verified this gives confidence that the overestimation of the ultimate failure load by 20% is due to boundary condition assumptions or the material and interface properties which in this case are taken from the literature. Further variation will be introduced due to the large scale of the panel manufactured increasing the likelihood of voids and similar defects which enhance crack initiation and propagation at the interface. Therefore the model's ability to replicate the buckling point, post-buckled response, mode I and II crack propagation and debond initiation has been verified both in it's individual components and in combination.

3. Parametric Assessment of Stiffener-Plate Debond Damage in Top-Hat Stiffened Panels

The verified model is used to assess the effects of debond damage at the stiffener plate interface. The effect of size of a central and offset debond for stiffened panels with a nominal and forced imperfection are assessed. Geometric parameters are investigated in terms of the stiffener height and stiffener spacing. Results are compared to similar studies on open section stiffeners to allow comparison of stiffener types. For all cases loads shown are scaled by the ultimate load of the intact case and the debond length is scaled as a percentage of the panel length.

3.1. Analysis of Damage Parameters

3.1.1. Analysis of Debond Size with Nominal Imperfection

The intact case is used as the reference case with the effect of central debonds sized from 50mm to 350mm at 50mm spacings.

The failure mechanism map is shown in figure 13 illustrating the change in ultimate strength, debond crack propagation, damage initiation, and panel, plate and stiffener buckling. The definition of these failure mechanisms is given in section 2.2. There is only minor deviation in the failure characteristics for debonds of 20% or less except for a gradual reduction in the local plate buckling load, although this has a nominal effect on the damage initiation and debond crack propagation.

Shear failure of the plate in the region of the anti-node lines, region corresponding to zero out-of-plane buckled deflection, is the dominant mode of failure for the intact case and small debonds. Debond crack propagation occurs simultaneously to the ultimate failure load however the developing shear damage in the plate and flange is considered to be the primary cause of ultimate failure. The intact case failure mechanisms are shown in figure 14; the plate buckles into three half sine waves with a positive inflection at the centre of the plate, damage initiates on the anti-node line (a) and develops across the width of the plate (b), the debond develops on the anti-node line on the inner flange edge and propagates across the flange just prior to ultimate failure (c).

At 26% the debond approaches the length of the half sine wave buckled mode and there is a significant reduction in the debond crack propagation load from 99.9% to 78.2% with a reduction in the ultimate strength to 94.7%. The debond crack propagates from the inner flange edge which enhances the plate deformation and aids damage propagation in the centre of the plate beneath the debond.

Debond crack propagation becomes dominant for debonds greater than 33%, which is greater than the length of the half sine wave inflection. Debond crack propagation occurs prior to the damage initiation load and is largely coincident with the stiffener buckling. This change in mechanism is caused by the inversion of the plate inflections, switching of the central inflection for positive to negative out-of-plane deflection. At this critical point the buckling mode shape shows a significant deflection beneath the debond and has altered the preferred buckling

mode of the plate. Instead of a positive inflection in the region of the debond, which pushes the debonded plate and flange together preventing mode I crack growth the negative inflection drives mode I opening at the debond crack tip on the inner corners. The untied flange also buckles away from the plate further enhancing the opening force. Shear damage initiates on the debonded flange and later on the anti-node lines of the supporting stiffener. A reduction in stiffener buckling, significant debond crack growth and a significant reduction in the ultimate strength to 73-74% of the intact case is observed.

For debonds increasing beyond this critical point a plateau exists where the ultimate strength remains greater than 60% of the intact ultimate strength. Material failure is observed in the centre of the flange and then on the anti-node line of the supporting stiffener. Ultimate failure is due to gross failure of the plate. The supporting stiffener is observed to debond only during the final collapse of the panel.

3.1.2. Analysis of Debond Size with Forced Imperfection

The failure mechanism map is shown in figure 15 for increasing debond size.

In contrast to the nominal imperfection case the intact case plate buckles into three half sine waves with a negative inflection at the centre of the plate although the failure mechanisms are similar to the nominal case.

The failure maps for the nominal imperfection case show a distinct change in modes at the critical debond size, 27%-33%. However the forced imperfection shows a more gradual change in characteristics as the debond size increases with the critical point at which crack propagation becomes significant between 0% and 6% debond. The crack propagation load shows a marked reduction from the intact case and then a steady reduction for increasing debond size. The ultimate strength rapidly decreases from the intact case to 20% debonds plateauing at 73% for larger debonds. The damage initiation load reduces between 13% and 33% debond although there is then a gradual rise between 33% and 46% debond. This increase represents localised damage in the flange-plate interface at the crack front. For large debonds the debond crack propagates up to the anti-node lines and failure is observed on the anti-node line of the intact stiffeners and in the central plate. Following a significant amount of failure in these regions the previously intact stiffener then debonds centrally as shown in figure 16 although this occurs post ultimate load.

With a forced imperfection plate buckling occurs at much lower loads for all debond sizes compared to those with a nominal imperfection. This is due to the change in the central inflection beneath the unsupported stiffener between the two cases which is illustrated in figure 17. However for debonds of 27% or greater both the nominal and forced imperfections form a negative inflection beneath the unsupported stiffener. The local plate buckling occurs at higher loads for the nominal case compared to the same debond size with a forced imperfection. The plate deformations beneath the flange, used to assess plate buckling, are shown in figure 18 for the intact cases and 40%, 300mm, debond for both a nominal and forced imperfection where the star shows the defined panel buckling point. The deflections for the intact case with forced imperfection remains negative,

resulting in a negative central inflection, and shows a more rapid change in the gradient of the out-of-plane deflection of the plate against end shortening compared to the nominal case. For the debond cases there is a more rapid decrease in the out-of-plane deflection for the forced imperfection compared to the nominal imperfection. Therefore the initial imperfection is shown to alter the plate deformations at lower loads resulting in a marked reduction in the plate buckling load for the forced imperfection, as expected.

For both imperfections debond crack propagation is always mixed mode although is mode I dominant where a negative inflection is present under the debond crack. When the debond crack is located over a positive inflection the mode II contribution is increased. The increased critical strain energy release rate in mode II compared to mode I means crack propagation is rarely the dominant failure mode

3.1.3. Effect of debond position

Debond position is investigated for small, 6.67%, medium, 20%, and large debonds, 40%. The location is represented as a ratio of the distance of the centre of the debond from the plate end against the total plate length.

For small debonds with both imperfections there is a similar range in ultimate load showing a 5.1% reduction. For the nominal imperfection this reduction is due to the flange debond located over the anti-node line allowing increased displacement and therefore stresses in this area accelerating the material degradation. The debond crack propagation for both imperfections is not a significant damage mechanism.

Figure 19 and 20 show the failure mechanism maps for medium debonds with a nominal and forced imperfection respectively. Comparing these figures shows the damage and ultimate load have similar trends for the positive and negative inflections which occur either side of the anti-node line, located at 0.35. A more gradual change in mechanisms occurs compared to small debonds with debond crack growth and ultimate failure occurring at increasing load as the debond moves towards the centre of the positive inflection for both imperfection cases. There is a reduction of 26-29% in the ultimate load and debond crack propagation load as the debond passes from the positive to the negative inflection. Debond crack growth occurs at lower loads for the panels with a forced imperfection. This may be due to the more pronounced plate deflections illustrated in figure 18. The clamped end provides reduced opening moment at the crack tip suppressing debond crack growth for debonds between the clamped end and the peak of the positive inflection. The buckling load and damage initiation on the anti-node lines remains relatively unaffected by debond location.

For small and medium debonds the buckled mode shape is unaffected by the debond in all locations which is not the case for large debonds. For a nominal imperfection the buckling mode shape changes from two to three half sine waves in the plates adjacent to the debonded stiffener if the debond is moved from the centre to the outer third of the plate. A reduction of 5% is observed in the ultimate load for a buckled mode shape of two half sine waves. This is due to a larger span between the anti-node lines which subsequently allows debonding

to a larger width, more significant deflections and damage to the web and table of the debonded stiffener. Asymmetric buckling modes caused by two half sine waves in the damaged bay and three half sine waves in the adjacent intact bay also introduce torsional bending to the intact stiffener contributing to shear failure in the web of the supporting stiffeners and promoting stiffener buckling.

Figures 21 and 22 show the failure mechanism maps for large debonds at varying locations for nominal and forced imperfections respectively. The range in deviation in ultimate load for the locations is similar for both imperfections. Damage initiation and buckling load remain relatively constant. The largest difference is seen in the panel buckling, stiffener buckling and debond crack propagation load. For a nominal imperfection there is little dependence on debond location however the forced imperfection is shown to postpone debond crack propagation and plate and stiffener buckling for offset debonds as the debond moves into the positive inflection.

The effect of debond position relative to the buckling mode shape can be seen to effect medium debonds only, affecting both the debond crack propagation and ultimate load.

3.2. Effect of Panel Topology

3.2.1. Stiffener Spacing

The effect of stiffener spacing is investigated for increased, 475mm, and reduced, 275mm, stiffener spacing compared to the reference case. For each panel the effect of central debonds with increasing size is investigated to assess their damage tolerance.

The intact ultimate strength is dominated by the stiffener second moment of area and is constant across the three spacings. The relationship between the ultimate strength and the debond size is similar for the three stiffener spacings; smaller debonds have little effect on the ultimate strength. At a critical debond size there is a marked drop in the ultimate strength followed by a plateau in ultimate strength for larger debonds. This critical debond size varies depending on the stiffener spacing occurring between 17% and 20% for the smaller stiffener spacing, 27% and 33% for the reference case and a more gradual change is observed between 17% and 27% for larger stiffener spacing.

The reference case and wide stiffener spacings show significant post-buckled strength with panel buckling occuring at 57.3% and 42.8% of ultimate load respectively. Whereas for the narrowest stiffener spacing panel buckling occurs at 99.9% followed by rapid collapse. For the narrowest stiffener spacing the ultimate strength is determined by stiffener buckling followed by material failure for the intact and debond crack propagation in the small damage cases. The panel's buckling mode may be affected by small debonds, 0-16%, causing switching between two and three half sine waves however, the ultimate load sees only a minor reduction compared to the intact case. For the reference and widest stiffener spacings the intact ultimate strength and small debond cases are driven by material failure which exaccerbates the stiffener buckling leading to ultimate collapse. For all stiffener spacings, at the critical point, the buckling

mode shape shows a significant deflection beneath the debond and has altered the preferred buckling mode of the plate resulting in mode I opening force at the crack tip and resulting in a significant reduction in the ultimate strength. For the narrowest spacing debond crack propagation leads to material failure and ultimate failure is due to debonding of the outer stiffener rather than stiffener buckling.

It is shown that for the reference and widest stiffener spacing that for small and medium debonds debond crack initiation does not propagate or diminish the ultimate strength of the panel significantly and that a 'no crack growth philosophy' results in conservative results.

3.2.2. Stiffener Height

For the intact case the failure mechanisms are similar to the reference case however stiffener debonding becomes more prominant for the squat stiffener and shear failure in the flange plate and web are critical for the tall stiffener. Figure 23 shows the effect of stiffener height on the failure mechanisms for the intact and large central debond cases. Considering the intact case there is a slight increase in local plate buckling, stiffener buckling, panel buckling and the damage initiation load as the stiffener height increases and a more pronounced increase in the ultimate load. Debond crack propagation is shown to increase from the squat to square stiffener but shows a decrease as the stiffener becomes tall. The increased second moment of area of the tall stiffener prevents the deformation of the stiffener causing an increased discrepency in the stiffness between the plate and the top-hat and a reduction in the debond crack propagation for the tall relative to the square stiffener for the intact case. The crack propagation is stable and the panel can carry increased load during crack propagation.

The pattern of failure mechanisms is similar between the stiffener ratios with a gradual reduction from the intact case to 27% debond, a marked reduction in ultimate strength between 27% and 33% and a plateau in debonds beween 33% and 47%. The tall stiffener shows a more marked reduction in the ultimate strength from the intact case to a debond size of 27% as debond crack propagation occurs at reduced loads compared to the square and squat cases. The three stiffener heights show a consistent trend of 75% ultimate load at the plateau. However the initial failure mechanisms such as local buckling, debond crack initiation, stiffener buckling and damage initiation occur at similar loads for these large damaged case.

3.2.3. Comparision of Stiffener Type

The effect of debonds in the study above is compared to the literature on open section stiffeners. This paper has shown, that for top top-hat stiffened reference case local plate buckling becomes significant at a critical load between 27% and 33% which is equivalent to the length of the half sine wave deformations for this panel. For debonds greater than this critical load debond crack propagation is driven by stiffener buckling. The effect of debond size was investigated by Yap [4] for 'T'-stiffeners. Yap's failure map for increasing debond size is shown in figure 24 for local buckling, global buckling and damage initiation.

Yap found debonds representing 10%-22% of the panel length to be the most critical as local buckling resulted in debond crack opening below the limit load, 66% of ultimate load. The critical point occurs at 10% debonds when local and global buckling occurs simultaneously. Yap found that for debonds greater than 22% the crack front was no longer the critical region and that the neighbouring stiffener also became critical but that the debond crack failed to propagate due to the thinness of the stiffener flange. Yap found that skin buckling away from the stiffener was not enough to initiate debond crack growth as the deformed state of the stiffener had a larger influence on debond crack growth. Top-hat stiffened panels have a different definition of global and local buckling due to the torsional rigidity of the stiffener, preventing stiffener tripping being coincident with global plate buckling. For top-hat stiffeners with a forced imperfection debond crack propagation may be initiated prior to stiffener buckling suggesting that manufacturing or material imperfections can cause debond crack propagation at reduced load depending on the debond location. No comparison to plate imperfection has been made by other authors.

This paper has shown that location dependence is relative to the buckled peaks and is critical where the global buckling peak deforms away from the stiffener. This confirms trends seen by Orifici et al. [7], Yap [4] and Wiggenraad et al. [5] for open section stiffeners. It is shown here that local buckling effects the global buckling for debonds representing 40% of the panel length however location dependence is still observed in the debond crack propagation load although it has little influence on the ultimate failure load. Yap [4] showed for T-stiffeners that debonds greater than 10% of the panel form local buckling prior to global buckling and that the location along the stiffener became less critical. Local buckling would influence the subsequent global buckling mode shape and the onset of failure. It is shown in this paper that this effect is less prominent in top-hat stiffened panels due to increased torsional rigidity preventing stiffener tripping.

The study of panel topology in this paper showed that stiffener height has little effect on the buckling load or damage tolerance which remains fixed as the ultimate strength increases with stiffener height. Stiffener spacing is shown to affect both the damage tolerance for large debonds and the critical debond size where the buckling mode shape shows a significant deflection beneath the debond and debond crack propagation becomes more prominent. Gadke et al. [10] also investigated the effect of top-hat stiffener panel topology on the damage tolerance with reference to the buckling load showing that geometric parameters could significantly affect the damage tolerance however where the damage tolerance was improved the load carrying capacity was decreased.

4. Conclusions

Top-hat stiffeners are used extensively in the aerospace, civil and marine industries due to their increased torsional rigidity compared to open section stiffeners. Debonds are commonly observed as defects or damage events. This paper presents an analysis investigating the effect of debond size and location

and geometric and manufacturing parameters on the residual capability of multi-stiffened composite structures. Inclusion of stiffener debonding as a damage mechanism is shown to be critical in assessing the ultimate load although it is only the dominant failure mode for key cases.

It is shown that top-hat stiffened panels with significant post-buckled strength exhibit a trend between the ultimate strength and the debond size. For small and medium debonds debond crack initiation does not propagate or diminish the ultimate strength of the panel significantly and a 'no crack growth philosophy' results in conservative results. As the debond grows and local buckling becomes significant debond initiation and growth become dominant in the collapse over material failure. For large debonds the plate anti-node lines provide limits to the debond crack growth length unless mode-switching is present. For the range assessed the ultimate strength remains greater than 60% of the intact case. Location dependence relative to the plate's buckling mode is observed only for medium debonds where the ultimate strength is reduced when positioned over the buckled negative inflection. In this paper the effect of debond position and panel topology has been investigated, other parameters to be investigated include the effect of the material properties, interface strength, multiple debonds, manufacturing variability and material failure associated with impact damage on the residual strength.

5. Acknowledgements

The authors would like to thank the UK Ministry of Defence and Lloyd's Register EMEA for their continued support and without whom this research would not have been possible. The authors acknowledge the use of the IRIDIS High Performance Computing Facility, and associated support services at the University of Southampton, in the completion of this work.

Table 1: Material & Cohsive Element Properties

	WRE580	UE500	Units	Reference
E_{11}	14910	26790	MPa	*
E_{22}	14910	5850	MPa	*
E_{33}	5850	5850	MPa	*
G_{12}	2110	2200	MPa	*
G_{13}	2110	2200	MPa	*
G_{23}	2110	2200	MPa	*
ν_{12}	0.119	0.272	-	*
ν_{13}	0.119	0.058	-	*
ν_{23}	0.119	0.058	-	*
S_{11T}	223.7	482.0	MPa	*
S_{11C}	171.5	308.0	MPa	*
S_{22T}	223.7	17.6	MPa	*
S_{22C}	171.5	87.8	MPa	*
S_{12}	23.2	24.2	MPa	*
t_{o_I}	17.6	-	MPa	Estimated from Manufacturer's Data
$t_{o_{II}}$	23.2	-	MPa	Juntikka and Olsson [13]
G_{IC}	1.21	-	kJ/m^2	Dharmawan et al. [23]
G_{IIC}	4.55	-	kJ/m^2	Dharmawan et al. [23]
η_{BK}	1.17	-	-	Calculated from Dharmawan et al. [23]
K_I	178000	-	MPa	Calculated using Turon et al. [24]
K_{II}	14910	-	MPa	Calculated using Turon et al. [24]
* Manufacturer's Data				

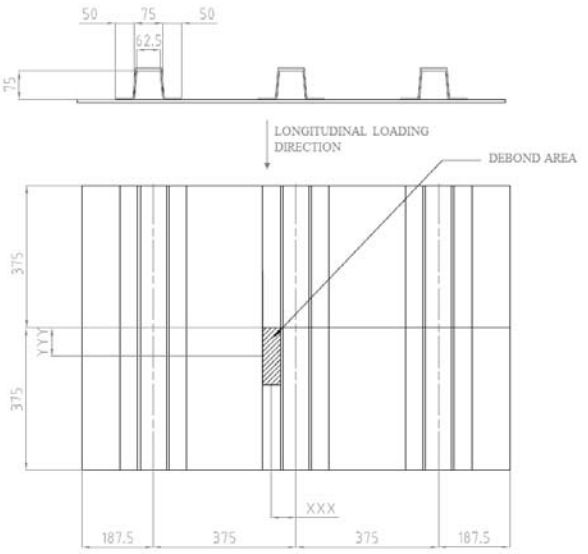

Figure 1: Multi Stiffened Panel Dimensions with Damage Position

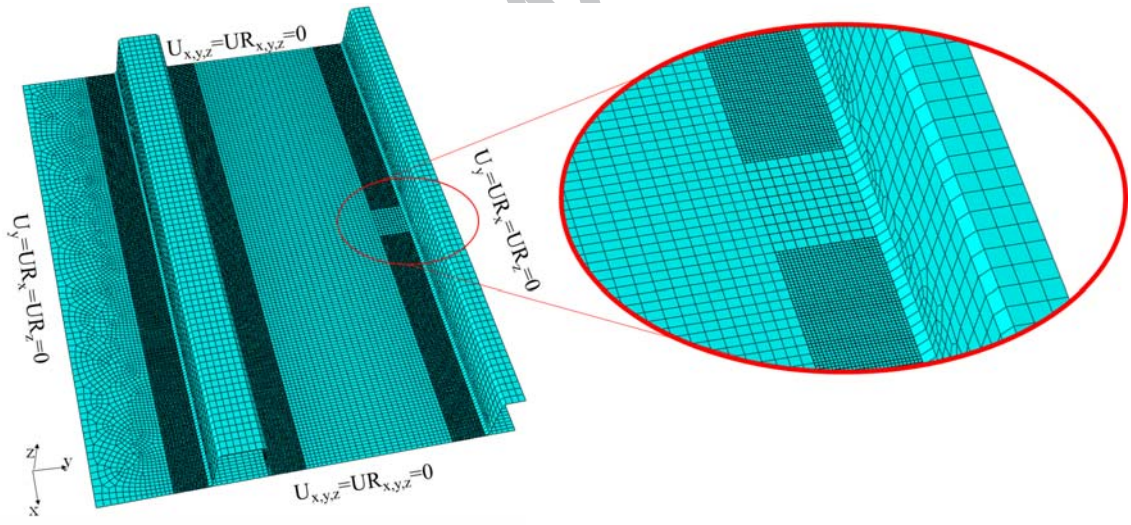

Figure 2: Model Boundary Conditions and Mesh Density

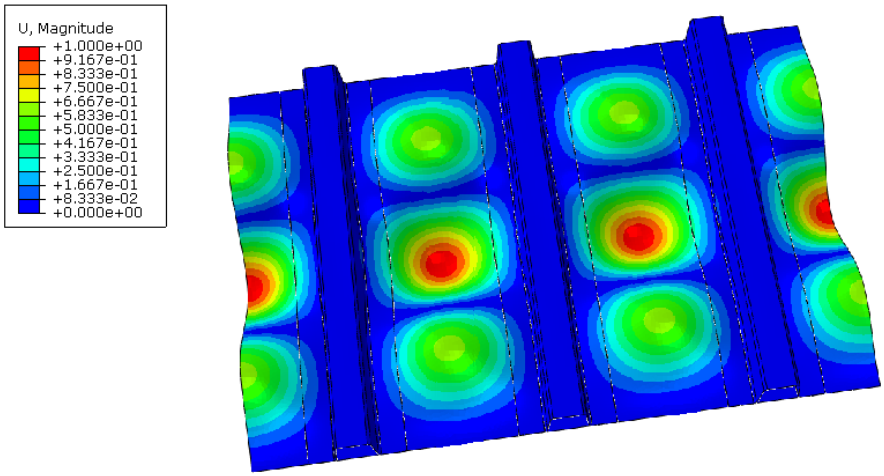

Figure 3: Applied Imperfection

Table 2: Progressive Damage Methodology

	Properties post failure
Fibre fracture	$E_1 = 0.01$
Inter Fibre Fracture: $\sigma_2 > 0$	$E_2 = 0.01E_2^0$, $G_{12} = 0.01G_{12}^0$
Inter Fibre Fracture: $\sigma_2 < 0$	$G_{12} = 0.01G_{12}^0$

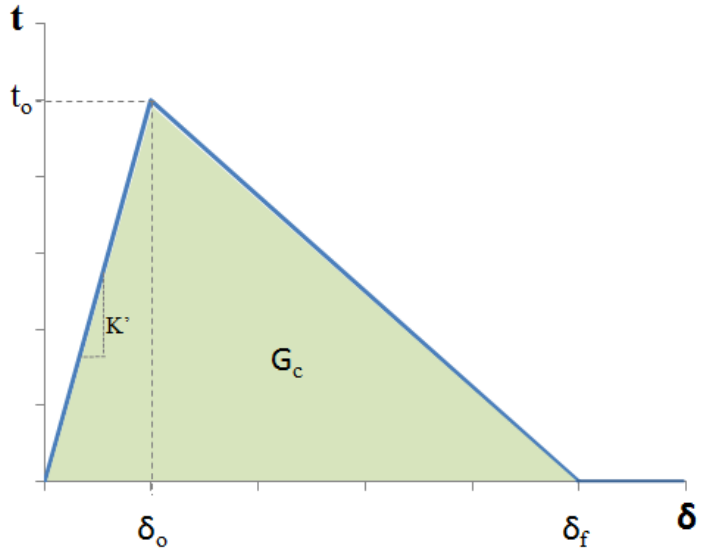

Figure 4: Constitutive linear softening relationship

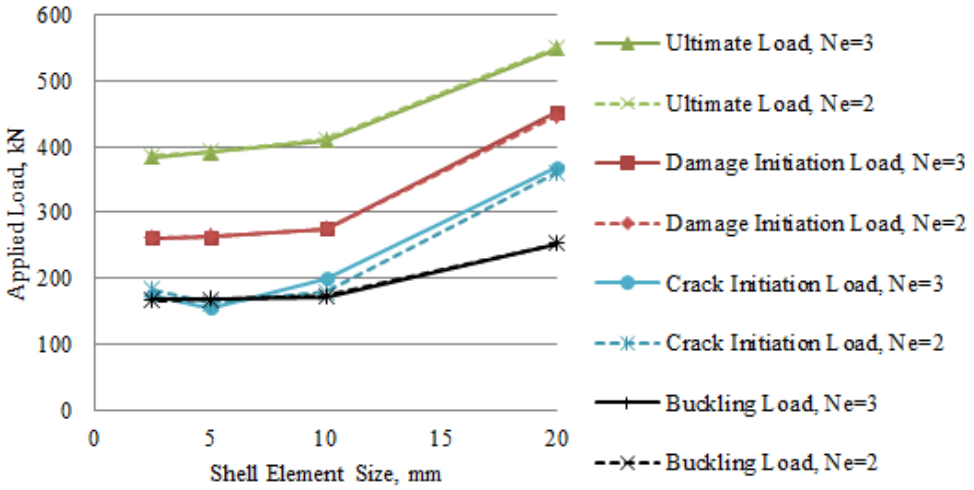

Figure 5: Convergence of Damaged Model

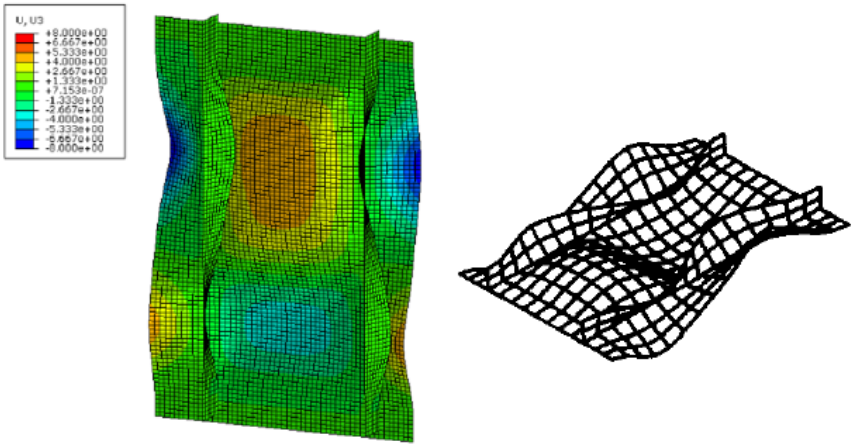

Figure 6: Comparison of Buckled Mode Shapes of Current Model and Kong et al. [17].

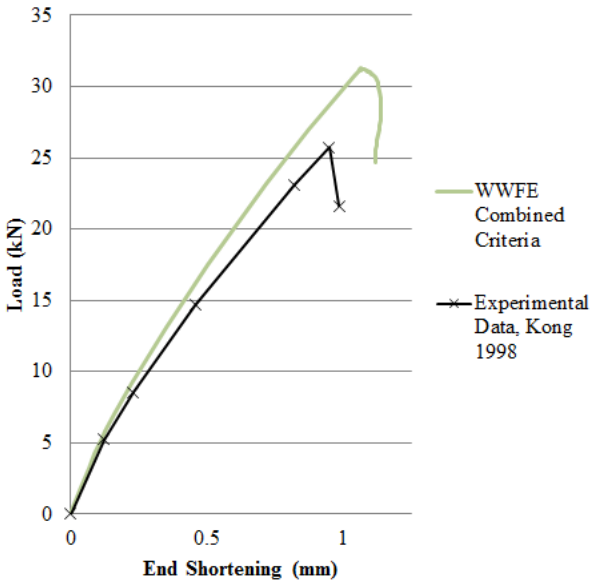

Figure 7: Stiffened Panel: Load End Shortening Response

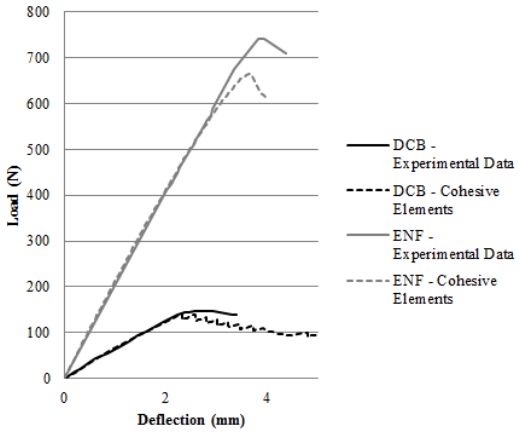

Figure 8: DCB and ENF: Load Deflection Response

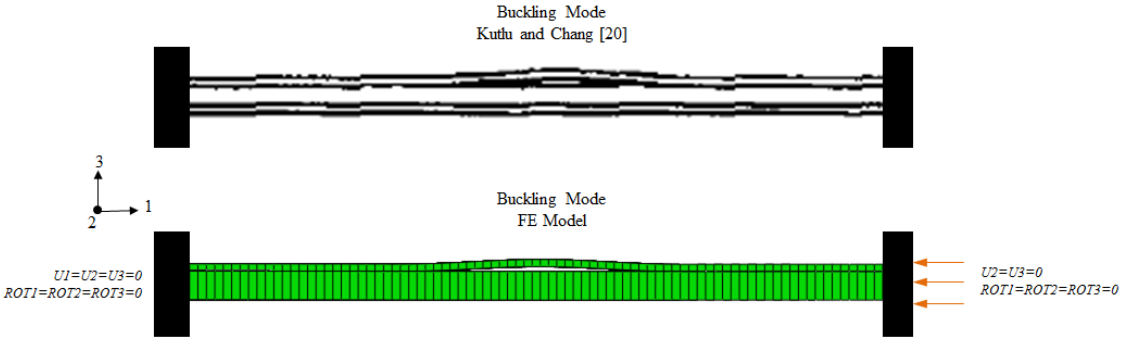

Figure 9: Through Width Delamination Model; Boundary Conditions & Comparison of Buckling Modes

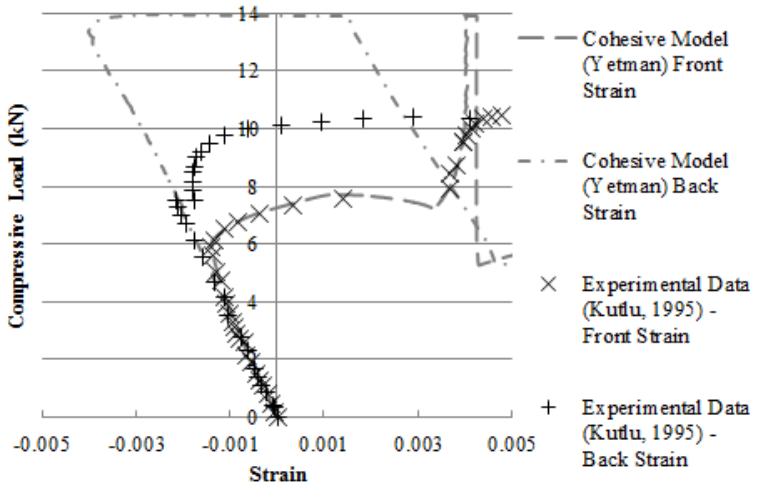

Figure 10: Through Width Delaminations: Load Vs Strain Response

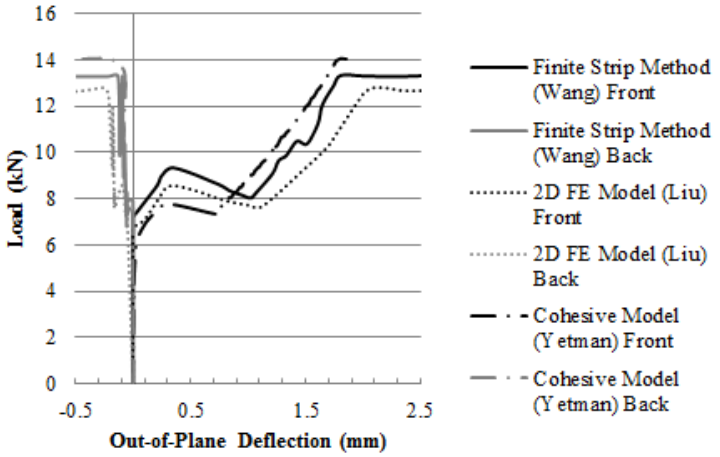

Figure 11: Through Width Delaminations: Load Vs Deflection Response

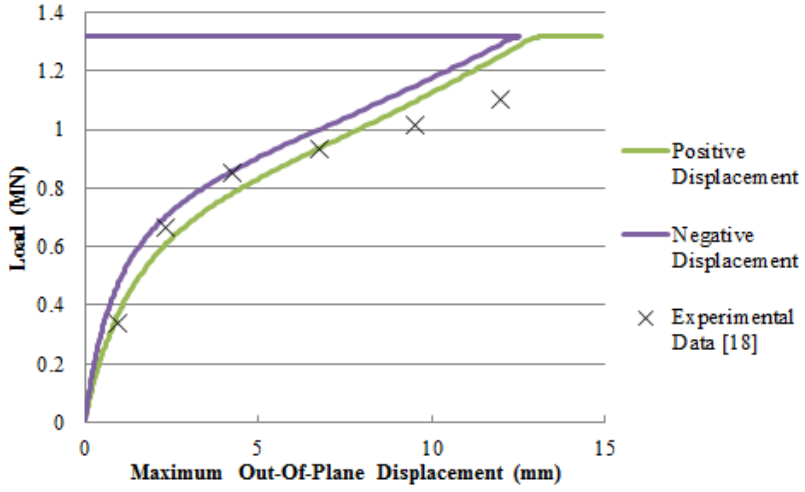

Figure 12: Top-Hat Stiffened Panel: Load Vs Out-of-Plane Displacement

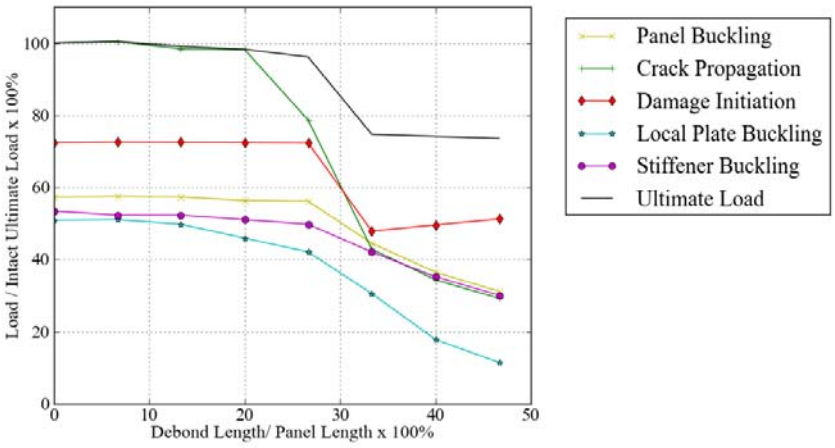

Figure 13: Failure Mechanism Map for Increasing Central Debond Size with Nominal Imperfection

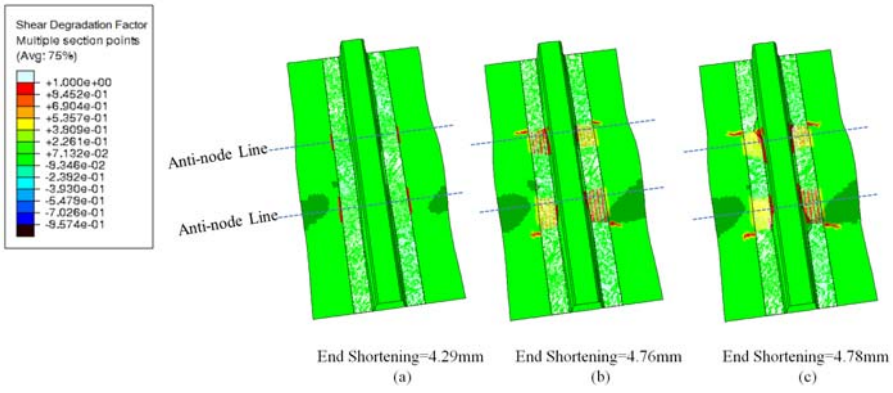

Figure 14: Shear Failure Development in the Intact Case

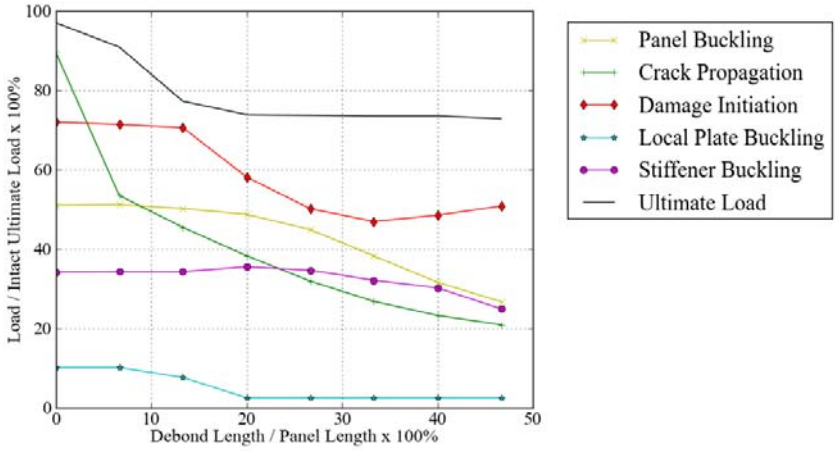

Figure 15: Failure Mechanism Map for Increasing Central Debond Size With forced Imperfection

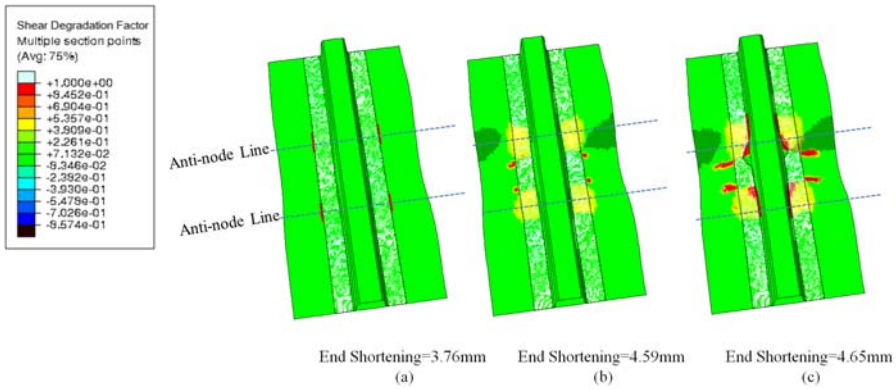

Figure 16: Shear Failure Development in the Forced Imperfection Intact Case

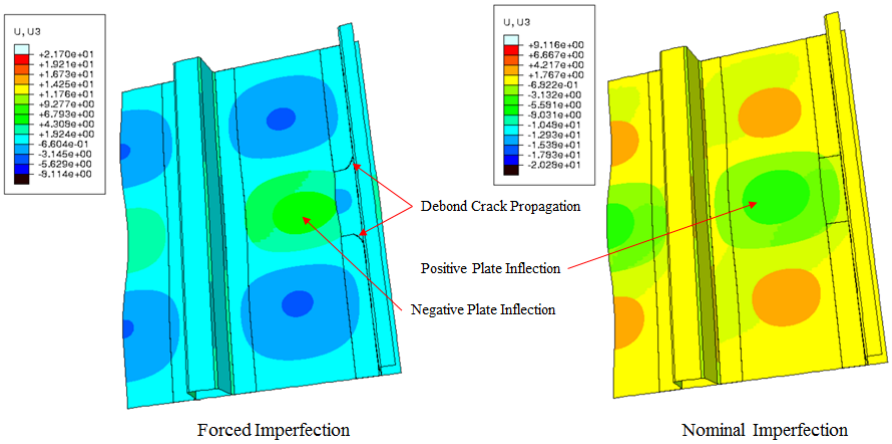

Figure 17: A Comparison of Plate Deflections for a 20% Debond at End Shortening 2.45mm

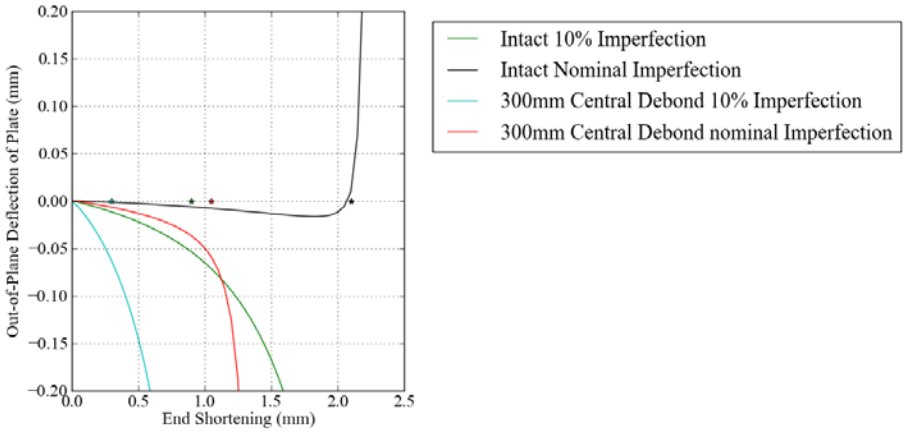

Figure 18: Comparison in Plate Deflection for nominal and forced imperfection

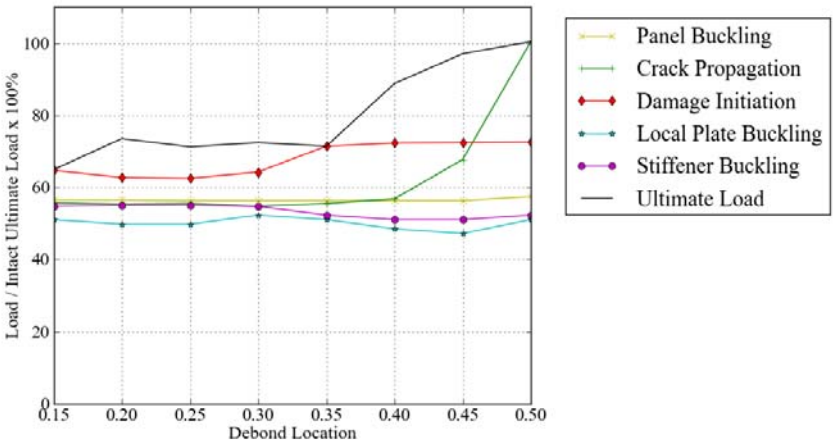

Figure 19: Failure Mechanisms for Offset Medium Debond with Nominal Imperfection

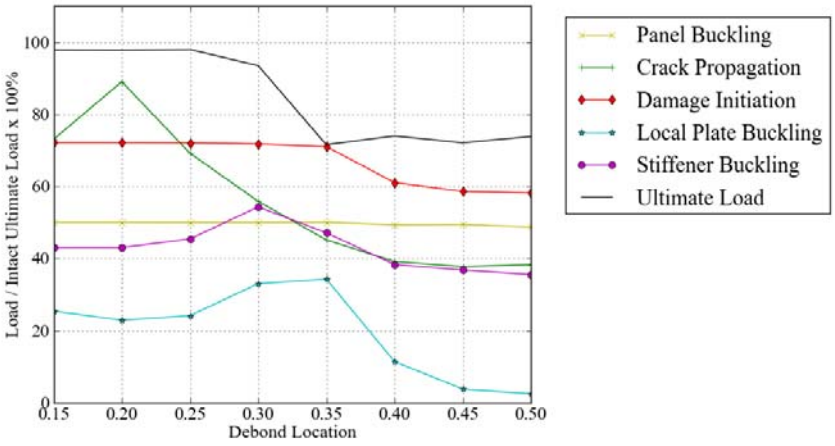

Figure 20: Failure Mechanisms for Offset Medium Debond with Forced Imperfection

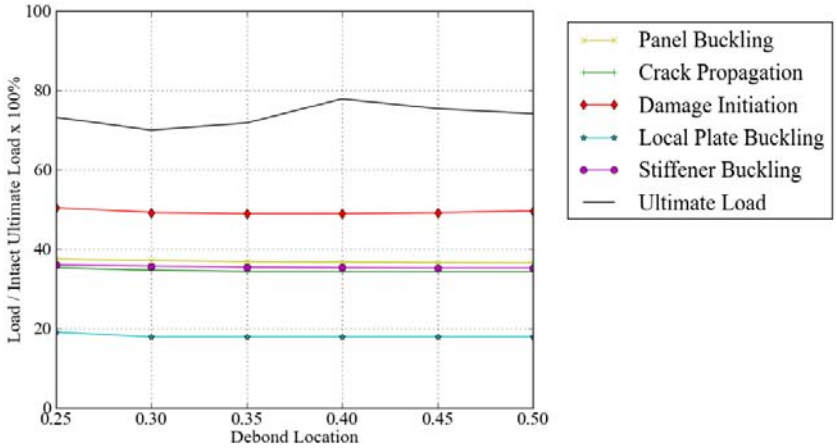

Figure 21: Failure Mechanisms for Offset large Debond with Nominal Imperfection

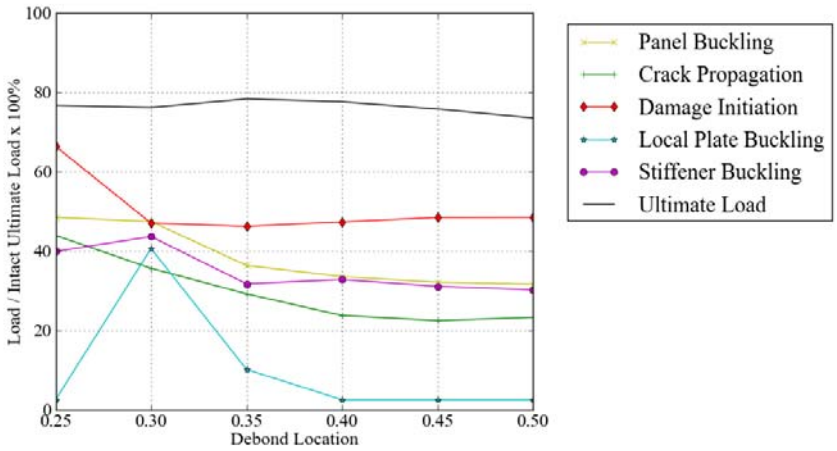

Figure 22: Failure Mechanisms for Offset large Debond with Forced Imperfection

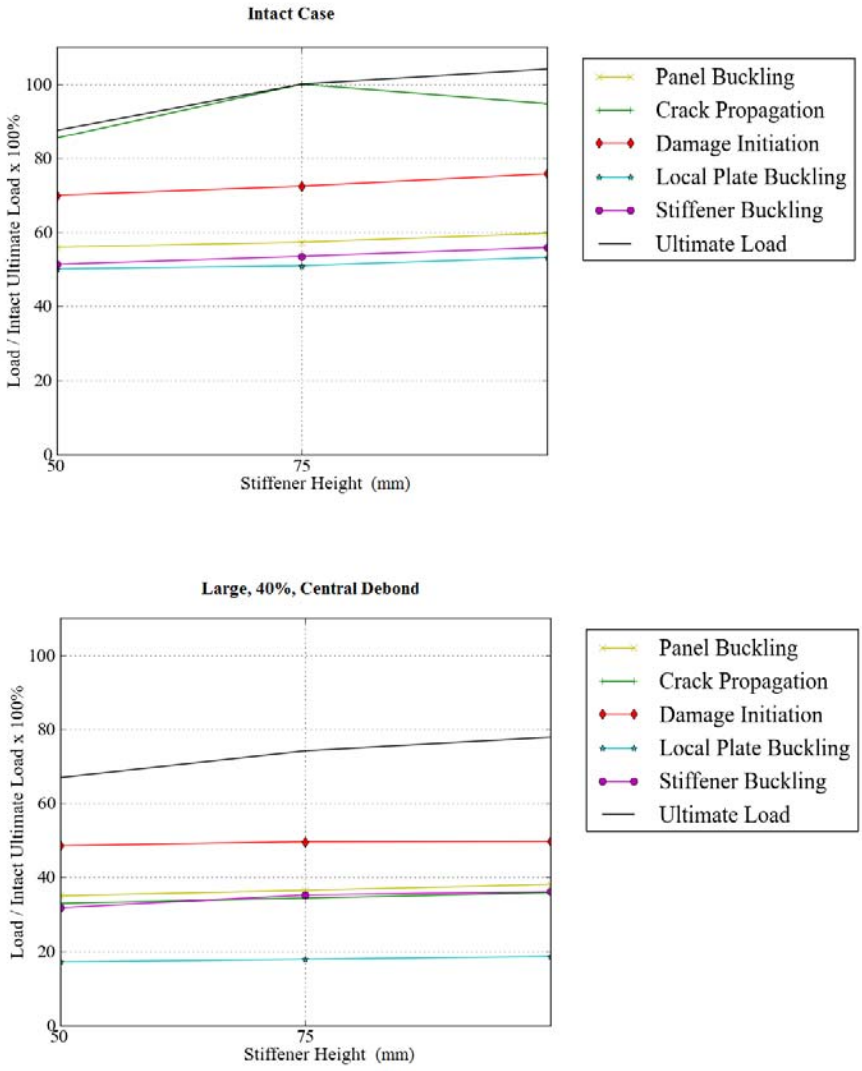

Figure 23: Assessment of Stiffener Height

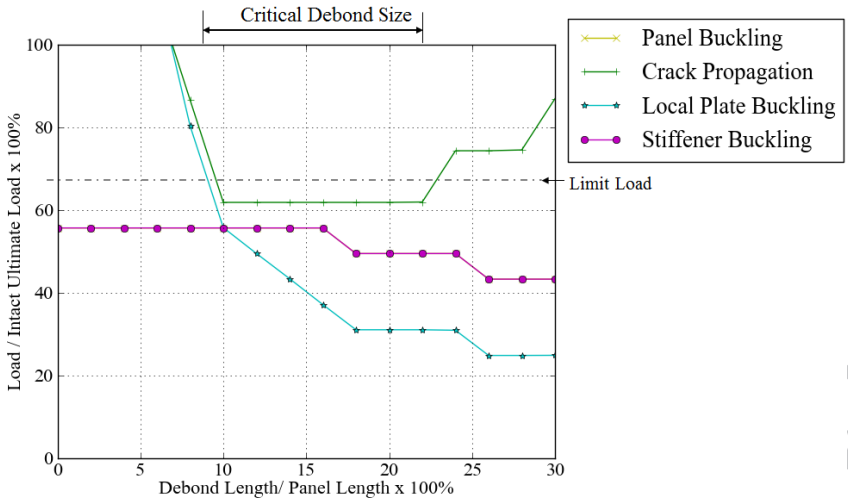

Figure 24: Yap [3] Analysis of Debond Size on T Stiffened Panel

References

[1] B. Falzon, Failure of thick-skinned stiffener runout sections loaded in uniaxial compression, Composite Structures 53 (2) (2001) 223–233, ISSN 02638223, doi:10.1016/S0263-8223(01)00006-X, URL http://linkinghub.elsevier.com/retrieve/pii/S026382230100006X.

[2] C. Meeks, E. Greenhalgh, B. Falzon, Stiffener debonding mechanisms in post-buckled CFRP aerospace panels, Composites Part A: Applied Science and Manufacturing 36 (7) (2005) 934–946, ISSN 1359835X, doi:10.1016/j.compositesa.2004.12.003, URL http://linkinghub.elsevier.com/retrieve/pii/S1359835X04003173.

[3] J. Yap, The analysis of skin-to-stiffener debonding in composite aerospace structures, Composite Structures 57 (1-4) (2002) 425–435, ISSN 02638223, doi:10.1016/S0263-8223(02)00110-1, URL http://linkinghub.elsevier.com/retrieve/pii/S0263822302001101.

[4] J. Yap, Influence of post-buckling behaviour of composite stiffened panels on the damage criticality, Composite Structures 66 (1-4) (2004) 197–206, ISSN 02638223, doi:10.1016/j.compstruct.2004.04.038, URL http://linkinghub.elsevier.com/retrieve/pii/S0263822304001308.

[5] J. Wiggenraad, E. Greenhalg, R. Olsson, Design and analysis of stiffened composite panels for damage resistance and tolerance, in: 5th world congress on computational mechanics; WCCM V, Vienna, July 2002, Vienna University of Technology, 1–493, URL http://scholar.google.com/scholar?hl=en&btnG=Search&q=intitle:Design+and+analysis+of+stiffene 2002.

[6] S. Suh, Compression behavior of stitched stiffened panel with a clearly visible stiffener impact damage, Composite Structures 62 (2) (2003) 213–221, ISSN 02638223, doi:10.1016/S0263-8223(03)00116-8, URL http://linkinghub.elsevier.com/retrieve/pii/S0263822303001168.

[7] A. C. Orifici, I. Dezaratealberdi, R. Thomson, J. Bayandor, Compression and post-buckling damage growth and collapse analysis of flat composite stiffened panels, Composites Science and Technology 68 (15-16) (2008) 3150–3160, ISSN 02663538, doi:10.1016/j.compscitech.2008.07.017, URL http://linkinghub.elsevier.com/retrieve/pii/S0266353808002716.

[8] A. Riccio, M. Giordano, M. Zarrelli, A Linear Numerical Approach to Simulate the Delamination Growth Initiation in Stiffened Composite Panels, Journal of Composite Materials 44 (15) (2010) 1841–1866, ISSN 0021-9983, doi:10.1177/0021998310364108, URL http://jcm.sagepub.com/cgi/doi/10.1177/0021998310364108.

[9] H. Suemasu, K. Kurihara, K. Arai, O. Majima, T. Ishikawa, Compressive property degradation of composite stiffened panel due to

debonding and delaminations, Advanced Composite Materials 15 (2) (2006) 139–151, ISSN 0924-3046, doi:10.1163/156855106777873897, URL http://www.tandfonline.com/doi/abs/10.1163/156855106777873897.

[10] M. Gadke, B. Geier, H. Goetting, Damage influence on the buckling load of CFRP stringer-stiffened panels, Composite Structures 36 (3) (1996) 249, URL http://www.csa.com/partners/viewrecord.php?requester=gs&collection=TRD&recid=199709C1D2375ED.

[11] J. Sumpter, Final review of Project Support Tasking DNA1217 - damage tomerance in FRP ship's structures, Tech. Rep., 1996.

[12] M. Benzeggagh, M. Kenane, Measurement of mixed-mode delamination fracture toughness of unidirectional glass/epoxy composites with mixed-mode bending apparatus, Composites Science and Technology 56 (4) (1996) 439–449, URL http://www.sciencedirect.com/science/article/pii/026635389600005X.

[13] R. Juntikka, R. Olsson, Experimental and modelling study of hail impact on composite plates, in: International Conference of Composite Materials, Edinburgh, 2009.

[14] C. S. Smith, Design of Marine Structures in Composite Materials, Elsevier, ISBN 1851664165, URL http://www.amazon.com/Design-Marine-Structures-Composite-Materials/dp/1851664165, 1990.

[15] G. Duvaut, J. Lions, Inequalities in mechanics and physics, Springer, Berlin, 1976.

[16] Z. Hashin, Failure criteria for unidirectional fibre composites, Journal of Applied Mechanics 47 (1980) 329–334.

[17] C.-W. Kong, I.-C. Lee, C.-G. Kim, C.-S. Hong, Postbuckling and failure of stiffened composite panels under axial compression, Composite Structures 42 (1) (1998) 13–21, ISSN 02638223, doi:10.1016/S0263-8223(98)00044-0, URL http://linkinghub.elsevier.com/retrieve/pii/S0263822398000440.

[18] J. R. Reeder, J. R. C. Jr, J. Crews, Mixed-Mode Bending Method for Delamination Testing, AIAA Journal 28 (7) (1990) 1270–1276.

[19] Z. Kutlu, F.-k. Chang, Composite panels containing multiple through-the-width delaminations and subjected to compression. Part II: experiments & verification, Composite structures 31 (4) (1995) 273–296, ISSN 02638223, doi:10.1016/0263-8223(95)00092-5, URL http://www.sciencedirect.com/science/article/pii/0263822395000933 http://linkinghub.elsevier.com/retrieve/pii/0263822395000925.

[20] P. D. Soden, A. Kaddour, M. J. Hinton, Recommendations for designers and researchers resulting from the world-wide failure exercise, Composites Science and Technology 64 (3-4) (2004) 589–604, ISSN 02663538, doi:10.1016/S0266-3538(03)00228-8, URL http://linkinghub.elsevier.com/retrieve/pii/S0266353803002288.

[21] P. Liu, J. Zheng, Recent developments on damage modeling and finite element analysis for composite laminates: A review, Materials & Design 31 (8) (2010) 3825–3834, ISSN 02613069, doi:10.1016/j.matdes.2010.03.031, URL http://linkinghub.elsevier.com/retrieve/pii/S0261306910001858.

[22] Y. Zhang, S. Wang, Buckling, post-buckling and delamination propagation in debonded composite laminates Part 2: Numerical applications, Composite Structures 88 (1) (2009) 121–130, ISSN 02638223, doi:10.1016/j.compstruct.2008.02.013, URL http://linkinghub.elsevier.com/retrieve/pii/S0263822308000494 http://www.sciencedirect.com/science/article/pii/S0263822308000500 http://dx.doi.org/10.1016/j.compstruct.2008.02.013.

[23] F. Dharmawan, G. Simpson, I. Herszberg, S. John, Mixed mode fracture toughness of GFRP composites, Composite Structures 75 (1-4) (2006) 328–338, ISSN 02638223, doi:10.1016/j.compstruct.2006.04.020, URL http://linkinghub.elsevier.com/retrieve/pii/S0263822306001516.

[24] a. Turon, C. Dávila, P. P. Camanho, J. Costa, An engineering solution for mesh size effects in the simulation of delamination using cohesive zone models, Engineering Fracture Mechanics 74 (10) (2007) 1665–1682, ISSN 00137944, doi:10.1016/j.engfracmech.2006.08.025, URL http://linkinghub.elsevier.com/retrieve/pii/S0013794406003808.